Solar Energy Vol. 27, pp. 51–65, 1981
Printed in Great Britain.

0038-092X/81/070051-15$02.00/0
Pergamon Press Ltd.

EFFECT OF VARIOUS DYES ON SOLAR DISTILLATION

ANIL K. RAJVANSHI

Solar Energy & Energy Conversion Laboratory, Department of Mechanical Engineering, University of Florida, Gainesville, FL 32611, U.S.A.

(*Received* 30 *July* 1979; *revision accepted* 28 *January* 1981)

Abstract—An analytical and experimental study of the effect of adding dyes to a solar distillation unit is reported in this paper. The analytical model developed treats the transient heat transfer inside the dye solution as one dimensional. The bulk fluid is discretized into layers with conduction, convection and radiation interactions occurring between them. Coupled with this is the energy exchange from the water surface to the glass cover of the still by convection, radiation and evaporation of water. Finite difference technique is used in solving the nonlinear partial differential equations. The experimental investigation is conducted using two identical stills. The dyes used are black napthylamine, red carmoisine and dark green, at various concentrations. Test results show that a dye solution is able to increase the distillate output by as much as 29 per cent (for black dye with 172.5 ppm concentration). Based on these tests, a method of calculating the percentage increase in evaporation effected by a specific dye over that from the control unit is developed. Among the dyes tested black napthylamine dye is found to be most suitable from two points of view: increased evaporation and no photochemical degradation. The agreement between the results from experiments and those from analytical model is excellent. The analytical model subsequently used to study the effect of ambient temperature, wind velocity and dye concentration on still productivity.

INTRODUCTION

Conventional solar distillation units have been studied for the past hundred years[1]. However, they suffer from certain drawbacks that have made them technically and economically unattractive for deployment on a large scale. These drawbacks are:

(1) Reduction in efficiency of distillation because of salt buildup in the basin. This requires constant flushing of the brine, thereby increasing the maintenance cost.

(2) Need of maintaining shallow depths, thereby requiring precise control of feed and thus increasing the capital cost of the system.

In order to overcome the above drawbacks, a novel concept of using water soluble dyes in deep basin distillation units is proposed in the present paper. By adding dye to the distillation unit, solar energy is absorbed in a very thin upper layer (≈2 cm), thus raising the surface temperature of the brine and increasing the productivity of the still. At the same time the problem of salt build up is reduced because salt can settle on the bottom of the basin without interfering in the solar radiation absorption near the surface.

The first part of the paper presents the analytical study, while the second part presents the experimental results. The third part of the paper presents the extrapolation on the analytical model in order to study the effect of variables such as ambient temperature, wind velocity and the concentration of dyes, on distillation productivity.

PART I

Figure 1 is the sketch of the model of the still used in the analysis. It shows the energy attenuation of a ray from the sun as it passes through the condensate-covered glass and into the dye-water mixture. In order to analyze the energy transfer process in the basin, the dye-water system has been divided into discrete layers of thickness Δx. The energy transfer among the layers is by conduction and convection while the energy input to them is by absorption of incident solar radiation. A detailed energy balance on the nth layer yields the following difference equation:

$$\left\{\int_{\lambda 1}^{\lambda 2} q^n_{\lambda,i}(t)\,d\lambda - \int_{\lambda 1}^{\lambda 2} q^n_{\lambda,1}(t)\exp(-\alpha_\lambda \Delta x^*)\,d\lambda\right\} A - \frac{k_e A(T_n^t - T_{n+1}^t)}{\Delta x} + \frac{k_e A(T_{n-1}^t - T_n^t)}{\Delta x} - (T_n^t - T_\infty^t)UP\,\Delta x = \rho_w A c_p \Delta x \frac{(T_n^{t+\Delta t} - T_n^t)}{\Delta t}. \quad (1)$$

In the above equation, the first two terms indicate the energy absorbed in a layer of thickness Δx^*. The absorption length is modified from Δx to Δx^* (Fig. 2) to account for the oblique angle of incidence of the solar radiation. The third and fourth terms in the above equation show the energy transfer with adjacent layers by conduction and convection. The last term on the l.h.s. of the equation is the heat transfer from the layer to the surroundings through the sides of the solar still. The term on the r.h.s. of the above equation is the rate of energy stored in the layer.

Figure 3 shows an experimentally determined typical temperature profile of the layers[2]. For convection heat transfer between the layers, the concept of equivalent conductivity is used[3]. The heat transfer between the

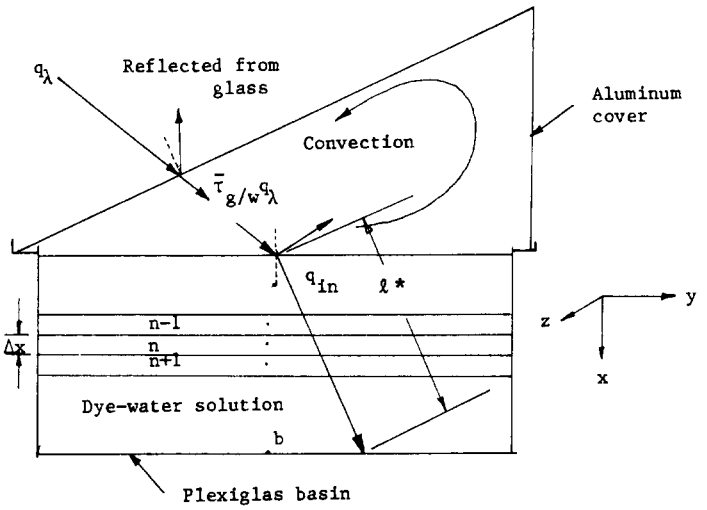

Fig. 1. Model of still used in analysis.

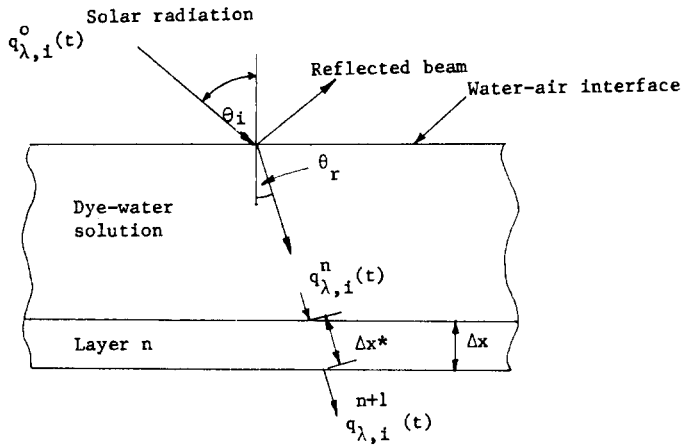

Fig. 2. Radiation transfer in the dye-water solution.

layers is then,

$$q_{conv} = \frac{k_e}{\ell}(T_{n,max} - T_s) \tag{2}$$

and the equivalent conductivity, k_e, is obtained by fitting the following straight lines to the data[3]:

$$\log_{10}\frac{k_e}{k_w} = \begin{cases} 0.3\log_{10}\mathrm{Ra}_\ell - 1; & \mathrm{Ra}_\ell > 2\times 10^4 \\ 0.25\log_{10}\mathrm{Ra}_\ell - 0.7; & \mathrm{Ra}_\ell \le 2\times 10^4. \end{cases} \tag{3}$$

Top surface

An instantaneous energy balance on the top surface yields:

$$\frac{k_e A(T_1^t - T_s^t)}{(\Delta x/2)} = h_m A(m_{is} - m_{ig})h_{fg} + h_c A(T_s^t - T_g^t) + \sigma F_e F_a A(T_s^4 - T_g^4) \tag{4}$$

where the first two terms on the r.h.s. give the heat transfer by evaporation and convection from the surface to the glass cover. The mass transfer coefficient h_m is calculated by analogy between heat and mass transfer[4]. In the temperature ranges encountered in the solar still, the Nussett number is given as;

$$\mathrm{Nu}_m = C(\mathrm{Gr}\,\mathrm{Sc})^{1/3} \tag{5}$$

which yields[2]

$$h_m = \rho D_{ij} C \frac{g(\Delta\rho/\rho)^{1/3}}{\nu_m D_{ij}} \tag{6}$$

and similarly heat transfer coefficient is given as,

$$h_c = C k_{w/a}\left[\frac{g(\Delta\rho/\rho)\,\mathrm{Pr}}{\nu_m^2}\right]^{1/3}. \tag{7}$$

The bouyancy factor $(\Delta\rho/\rho)$ in the above equations is given by[2]

$$\frac{\Delta\rho}{\rho} = 2\left(\frac{1-x}{1+x}\right) \tag{8}$$

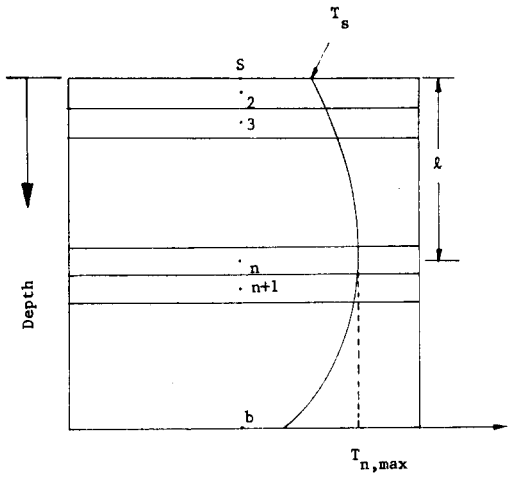

Fig. 3. Temperature profile of the layers.

where

$$x = \frac{T_g}{T_s}\left[\frac{P_{ws} + (P_{atm} - P_{ws})(M_{air}/M_w)}{P_{wg} + (P_{atm} - P_{wg})(M_{air}/M_w)}\right]. \quad (9)$$

Finally the mass transfer driving potential $(m_{is} - m_{ig})$ is given by [4]

$$(m_{is} - m_{ig}) = \frac{P_{ws}M_w}{P_{ws}M_w + (P_{atm} - P_{wg})M_{air}} - \frac{P_{wg}M_w}{P_{wg}M_w + (P_{atm} - P_{wg})M_{air}}. \quad (10)$$

Bottom surface

An instantaneous energy balance on bottom surface yields;

$$A\left\{\int_{\lambda_1}^{\lambda_2} q^0_{\lambda,i}(t)\exp(-\alpha_\lambda \ell^*)\,d\lambda\right\} = \frac{k_e A(T_b^t - T^t_{b-1})}{\Delta x} + \frac{k_{pg}A(T_b^t - T^t_{b,out})}{\Delta x_{pg}} \quad (11)$$

where $T^t_{b,out}$ is the temperature of the outside surface of the basin and T^t_{b-1} is the temperature of the layer $(b-1)$ (the bottom layer is b).

Energy exchange with the still cover

The r.h.s. of eqn (4) gives the rate of energy into the glass and aluminum cover. This energy must be given up to the environment. At the same time there is a small amount of solar radiation absorbed by the glass cover. Thus the temperature of the cover is given by:

$$\sigma F_e F_a A(T_s^4 - T_g^4) + h_m A(m_{is} - m_{ig})h_{fg} + h_c A(T_s^t - T_g^t) + \alpha_g A_g q(t) - h_0 A_c(T_g^t - T_\infty^t) - \sigma F_{ec}F_{ac}A_c \times (T_g^4 - T_{sky}^4) = \rho_g c_{pg} A_g \Delta x_g \frac{(T_g^{t+\Delta t} - T_g^t)}{\Delta t} + \rho_{al} c_{pal} A_{al} \Delta x_{al} \frac{(T_{al}^{t+\Delta t} - T_{al}^t)}{\Delta t}. \quad (12)$$

Experimentally it was observed that during daytime the temperature of the aluminum back plate was greater than the surface temperature of water. Thus no condensation took place on the back plate. At night, however, there was condensation at the aluminum plate but its temperature was equal to that of the glass cover. Moreover an order of magnitude analysis of eqn (12) shows that the storage term in the aluminum is negligible. Thus all the temperatures T_{al} in the above equation can be considered as T_g. This yields;

During daytime

$$\sigma F_e F_a A(T_s^4 - T_g^4) + h_m A(m_{is} - m_{ig})h_{fg} + h_c A(T_s^t - T_g^t) + \alpha_g A_g q(t) - h_0 A_g(T_g^t - T_\infty^t) - \sigma F_{eg}F_{ag}A_G(T_g^4 - T_{sky}^4) = \rho_g c_{pg} A_g \Delta x_g \frac{(T_g^{t+\Delta t} - T_g^t)}{\Delta t}. \quad (13)$$

During nighttime

$$F_e F_a A(T_s^4 - T_g^4) + h_m A(m_{is} - m_{ig})h_{fg} + h_c A(T_c^t - T_g^t) - h_0 A_c(T_g^t - T_\infty^t) - \sigma F_{ec}F_{ac}A_c(T_g^4 - T_{sky}^4) = \rho_g c_{pg} A_g \Delta x_g \frac{(T_g^{t+\Delta t} - T_g^t)}{\Delta t}. \quad (14)$$

Note the change in cover areas for day and night in eqns (13) and (14) respectively.

Incident solar radiation

The incoming spectral solar radiation reaching the dye-water surface is considered having wavelengths in the range of 0.3–2.0 μm [5]. To facilitate computation, it has been smoothed by fitting a polynomial in the above range. Thus the radiant flux is

$$q_\lambda = \begin{cases} 7.5\lambda - 2.25;\ 0.3\ \mu m \le \lambda \le 0.5\ \mu m \\ 3.97\exp(-1.95\lambda);\ 0.5\ \mu m \le \lambda \le 2.0\ \mu m. \end{cases} \quad (15)$$

The spectrum given by eqn (15) is the maximum radiation available at the solar noon on a clear day and will thus have to be modified for different times of the day. Thus the spectral radiation at any time is,

$$q_\lambda(t) = \zeta(t) q_\lambda \quad (16)$$

where

$$\zeta(t) = \left[\frac{q(t)}{\int_{0.3}^{2.0} q_\lambda\, d_\lambda}\right] \quad (17)$$

The radiation passing the water–air interface is given as,

$$q^0_{\lambda,i}(t) = \bar{\tau}_{g/w}(1 - r)q_\lambda(t) \quad (18)$$

where the reflectance r is given by the Fresnel equation,

$$r = \frac{1}{2}\frac{\sin^2(\theta_i - \theta_r)}{\sin^2(\theta_i + \theta_r)}\left[1 + \frac{\cos^2(\theta_i + \theta_r)}{\cos^2(\theta_i - \theta_r)}\right] \quad (19)$$

and

$$\frac{\sin\theta_i}{\sin\theta_r} = \frac{n_2}{n_1}. \tag{20}$$

It has been assumed that over the wavelength range of 0.3–2.0 μm the index of refraction for dye solution remains constant and that it is equal to that of water. This assumption seems to be valid since the concentrations of the dye used in the present study are very small (maximum concentration is 172.5 ppm).

METHOD OF SOLUTION

The depth of the still is 26.7 cm and, with grid size of $x = 2.54$ cm, there are 11 nodal equations and two boundary conditions for the top and bottom surfaces. A computer program was written to solve these 13 nodal equations for the dye-water and one equation for the glass cover simultaneously. The finite difference technique was used in solving these equations. Since an explicit method of solution was used in solving them the time interval Δt was carefully chosen so as to avoid unstable solutions. The input to the program included ambient temperature-time history, outside wind velocity and solar radiation data. This data was obtained for the days of the test. The coefficient C (eqns 6 and 7) was determined experimentally[2]. The absorption coefficient α_λ of the dye and average transmittance of the condensate covered glass $\bar{\tau}_{g/w}$ was obtained experimentally[2] and these values were used in the computer program. The output from the program was the temperature-time histories of various layers of dye solution and glass cover and distillate histograms.

PART II

EXPERIMENTAL RESULTS AND DISCUSSION

Two identical deep basin solar distillation units were constructed for testing. One of these was used as a control while the other was used for testing the effect of dyes. The overall dimensions of each basin were $1.22 \times 1.22 \times 0.305$ m[2]. The dyes used in the present study were water soluble and supplied by GAF Corp. They were:

(1) Napthylamine 10 BR (black).

(2) Carmoisine BA Ex (red).

(3) Mixture of 33 per cent by weight of each of the following dyes: neptune BR (blue), carmoisine BA Ex (red) and tartrazine C extra (yellow). This mixture resulted in dark green dye.

Table 1 shows the concentration of the dyes used and the duration of the tests. The absorption spectrum of the dyes was obtained experimentally[2] (Fig. 4). The absorption spectrum of the dyes between 0.75 and 2.0 μm followed exactly that of water[2]. After the completion of the tests the spectrum of the dyes was again analysed for possible photochemical and thermal degradation. Red and green dyes did show appreciable degradation (Fig. 4), while the black napthylamine did not exhibit any degradation for the duration of the experiment.

TEMPERATURE-TIME HISTORY OF THE STILL

Figure 5 shows a typical measured temperature-time history of black dye. A large number of such temperature-time histories were measured daily over the duration of experiments[2] of which Fig. 5 is representative and thus a discussion on it is sufficient. The top layer (1.25 cm below the water surface) temperature reaches a maximum of 43.3°C around 2:30 p.m. (EST) whereas the maximum solar radiation is reached around 12:40 p.m. This lag is because of mass of dye-water system. The temperature of the bottom layer, on the other hand, continues to rise, since there is heat conducted from the top layers during daytime and also a small portion of incident solar radiation is absorbed by it. After about 3:30 p.m. the top layer temperature falls rapidly, both because of rapid evaporation of water from the surface as well as the cooling of environment. At around 3:30 a.m. the bottom layer temperature and top layer temperature merge. This is because after this time the convection currents are set up and the whole system loses heat as a single mass. The intermediate layers also follow the same trend. It can also be seen from this figure that the condensation on the back aluminum plate takes place after 4:30 p.m.

The bottom layer temperature and the time at which it merges with the top layer temperature is an indication of the optical depth of the dye-water system. This point can be seen in Fig. 6 where the temperature-time history of

Table 1. Duration of tests

Dye	Concentration (ppm)	Duration of Test
Carmoisine (Red)	50.0	11/10/77 - 12/08/77
	100.0	12/10/77 - 02/14/78
Napthylamine (Black)	50.0	02/16/78 - 03/28/78
	172.5	03/29/78 - 04/24/78
Dark Green	50.0	04/26/78 - 08/13/78
	100.0	08/15/79 - 09/21/78

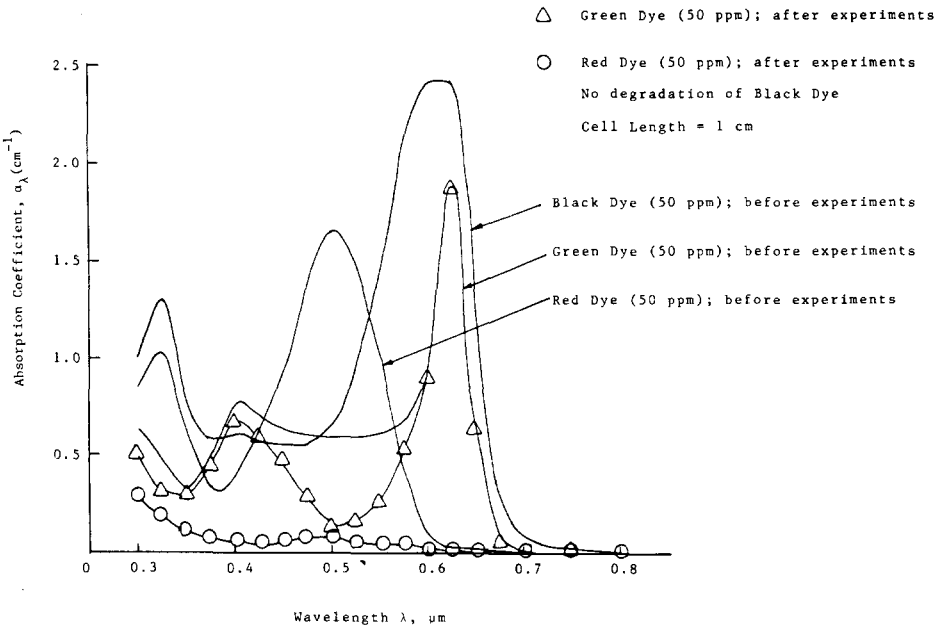

Fig. 4. Absorption spectrum of various dyes.

black dye and that of controlled still are plotted. The time of merging for water is around 9:30 p.m. as compared to 1:30 a.m. for that of black dye. This is because higher absorption of solar radiation in a dye solution delays the merging of top and bottom layer temperatures, since the convection currents in the solution are set up later in the day. This point can be further amplified by examining the solar energy absorbed by different dyes for various depth of solution. Figure 7 shows the calculated absorption of solar energy for different dyes. These calculations for different depths are based on the first two terms of eqn (1). Pertinent data on water is obtained from Hale and Querry[6].

Productivity of still

One consequence of the temperature-time history explained above can be seen in the distillate output of the two stills (see Fig. 8 for the distillate histogram). Since the top layer temperature of the dye is higher than that of the top layer in the control unit during daytime, the distillate output is higher for this as compared to that from control unit. Measurements show that around 60 per cent of the total distillate output for the dye system takes place during daytime as compared to that from the control unit where only 30 per cent occurs during daytime and 70 per cent during the night. It can also be seen that because of higher brine temperature of the control

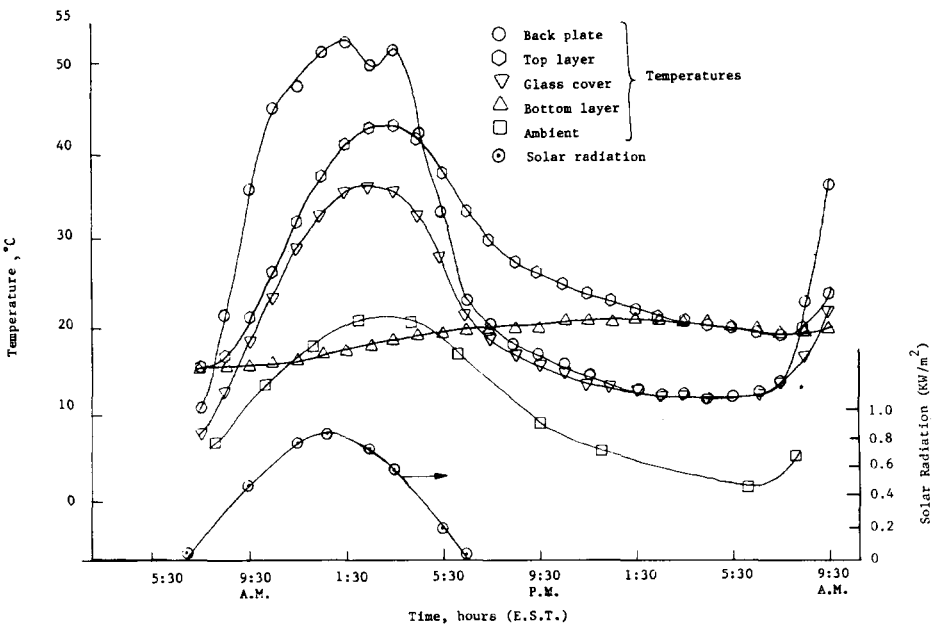

Fig. 5. Temperature-time history of black dye (50 ppm); 6 March 1978.

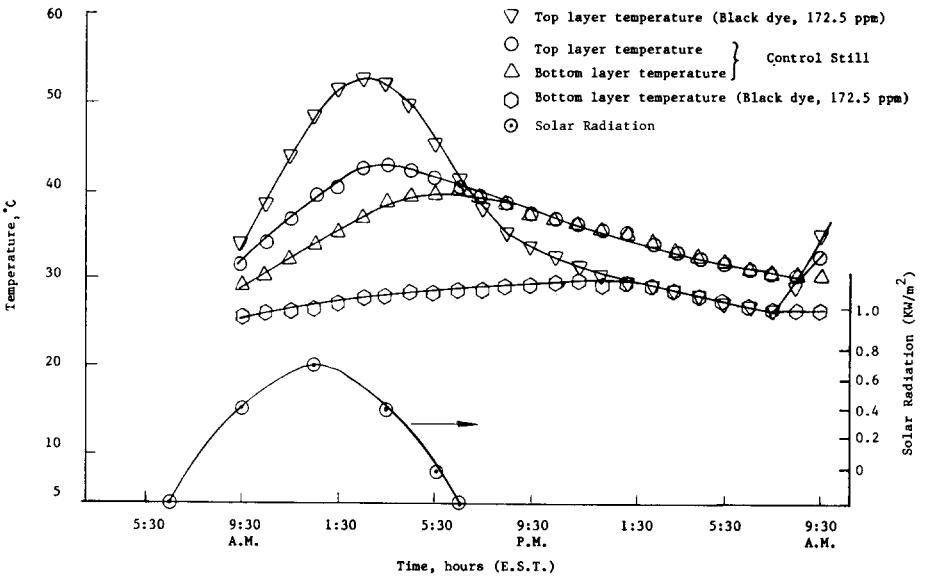

Fig. 6. Temperature-time history of the two stills; 31 March 1978.

unit at night, greater heat loss occurs from the bottom and the sides of the still, as compared to that from the still with dye. This results in lower efficiencies for deep basin still (with water only). Table 2 shows the comparison of efficiencies between the control unit and the dye unit, for various days.

It should be pointed out that the distillate output depends both on the brine surface temperature and the temperature difference (ΔT) between the brine surface and the glass cover[9]. Figure 9 shows the correlation between h_{evap} and T_s, where h_{evap} is given by the following equation:

$$h_{evap} = \frac{h_m(m_{is} - m_{ig})h_{fg}}{\Delta T}. \tag{21}$$

Thus with higher T_s there is greater evaporation. However the driving potential ΔT controls evaporation. This point will be further amplified in the next section.

A much more meaningful relationship for a researcher in the area of solar distillation is between distillate output and T_s. Figure 10 shows this relationship. It should be

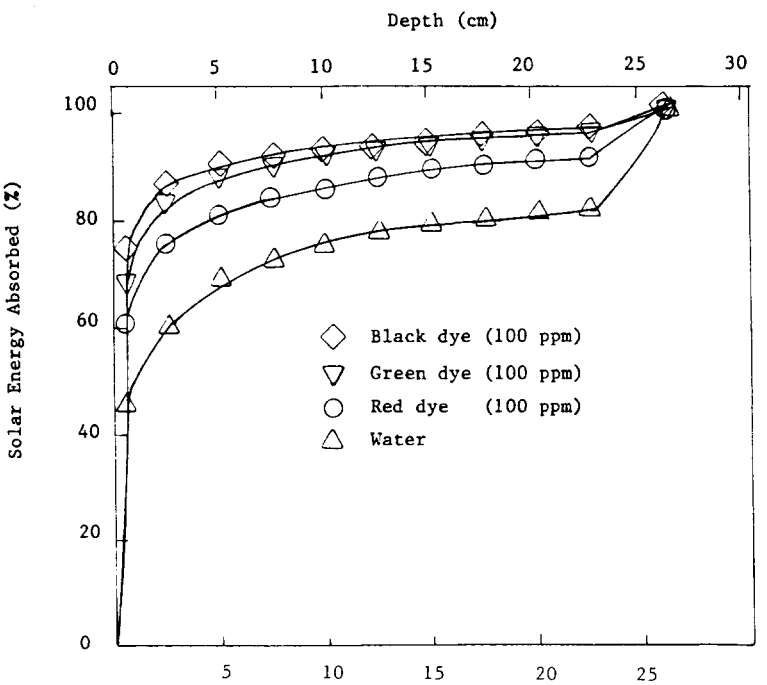

Fig. 7. Percentage of solar energy absorbed with depth of solution; 14 April 1978 at 12:30 p.m. (EST).

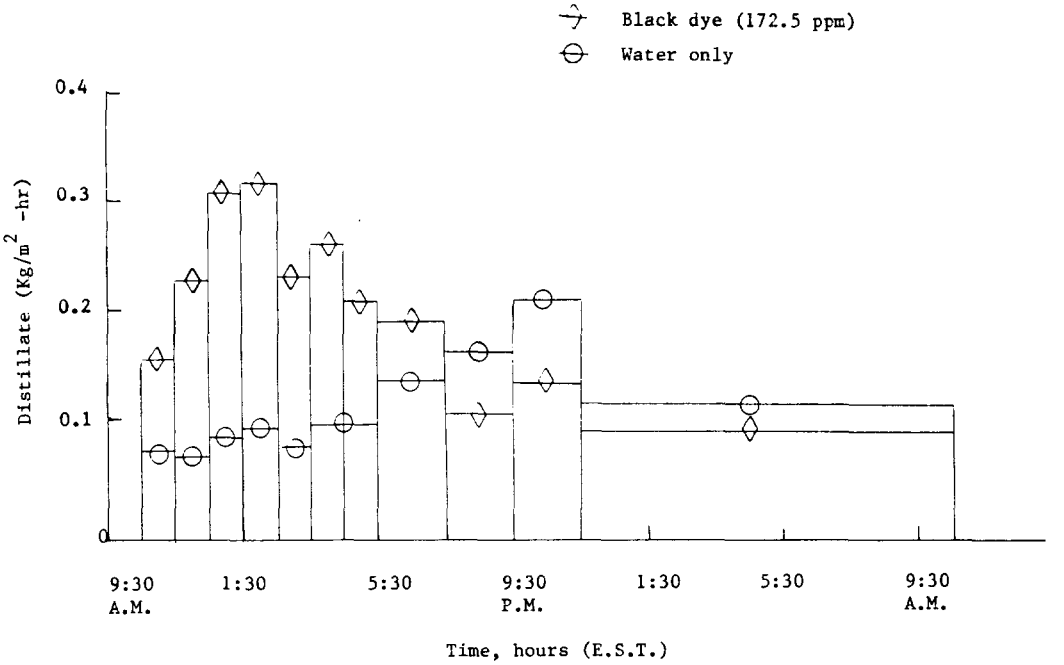

Fig. 8. Distillate histograms from two stills; 15 April 1978.

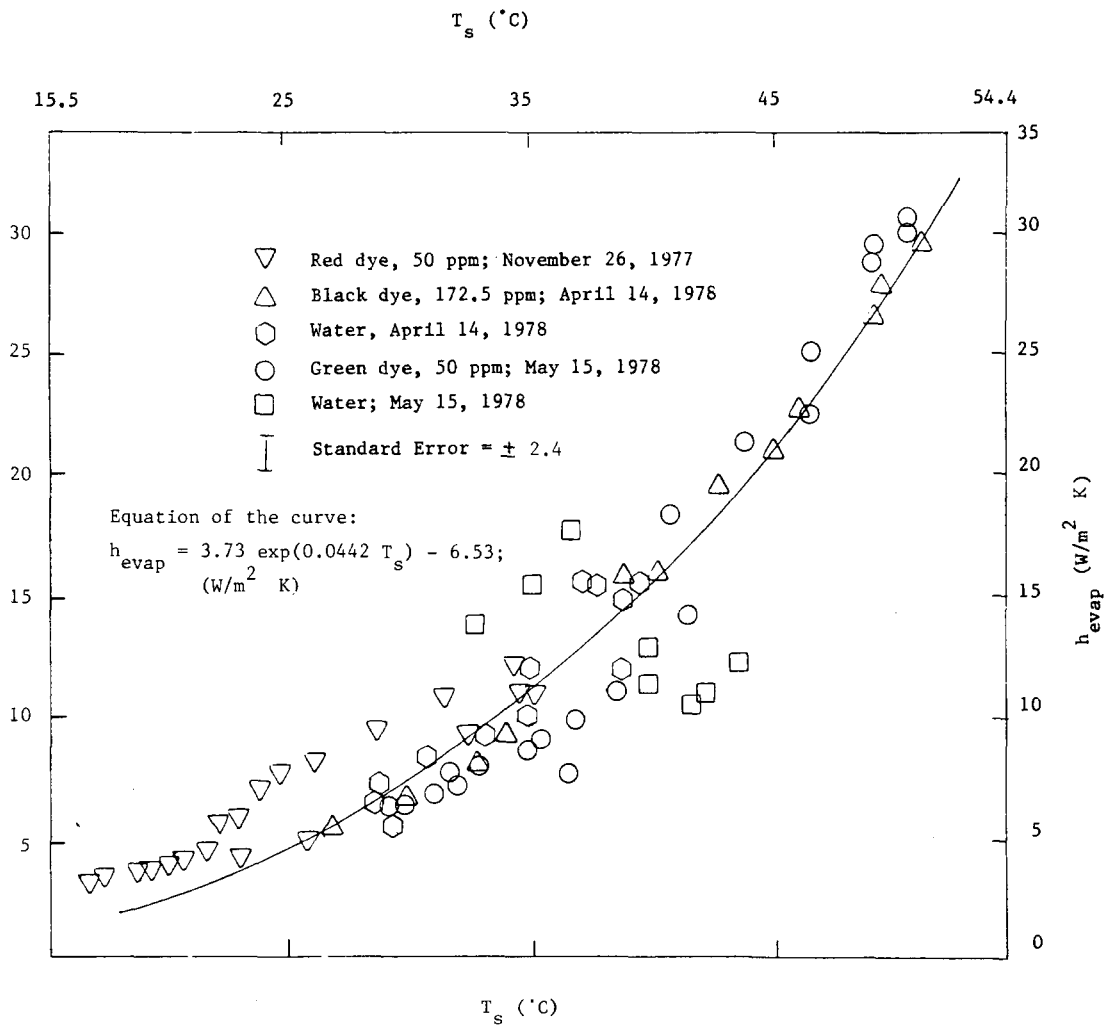

Fig. 9. Correlation between h_{evap} and T_s.

Table 2. Comparison of dyes (experimental)

Date	Dye	Conc. ppm	Solar Rad.[1] kJ/day	Distillate (dye) kg	Distillate (control) kg	Efficiency[2] η_d (dye)	η_c	Percent Diff.[3]
November 26/77	Red	50	21830	3.6	3.35	38.3	35.7	7.4
January 10/78	Red	100	20410	3.05	2.55	34.8	27.4	19.9
March 17/78	Black	50	33238	4.31	3.71	30.1	26	15.9
March 31/78	Black	172.5	33086	5.31	4.53	37.34	31.8	17.1
April 14/78	Black	172.5	35864	5.60	4.35	36.2	28.1	28.8
April 15/78	Black	172.5	35085	5.54	4.37	36.77	28.9	26.9
May 15/78	Green	50	40654	5.55	4.84	31.8	27.7	14.8
August 22/78	Green	100	32598	5.19	4.64	37	33.1	12.0

[1]Solar Radiation (kJ/day) = (kJ/m^2-day) x 1.486 m^2

[2]Efficiency η = $\frac{\text{kg of distillate x 2321 (kJ/kg)}}{\text{Total Solar input}}$

[3]Percent Difference = $\frac{\text{Distillate (dye) - Distillate (control)}}{\text{Distillate (control)}}$ x 100

pointed out that the above relationships (Figs. 9 and 10) are only valid for passive type solar distillation units. If the glass temperature is changed artificially then they are not valid[9, 2].

†Nearly clear day is arbitrarily defined as a day on which sun produces shadow for nearly 70 per cent of the time.

Comparison of different dyes

The dyes were compared to each other by comparing the distillate output from dye system m_d, against that from the control still m_c.

Various regression lines were drawn for the test dyes[2]; Fig. 11 shows one such representative comparison. The data used in these plots are for nearly clear†

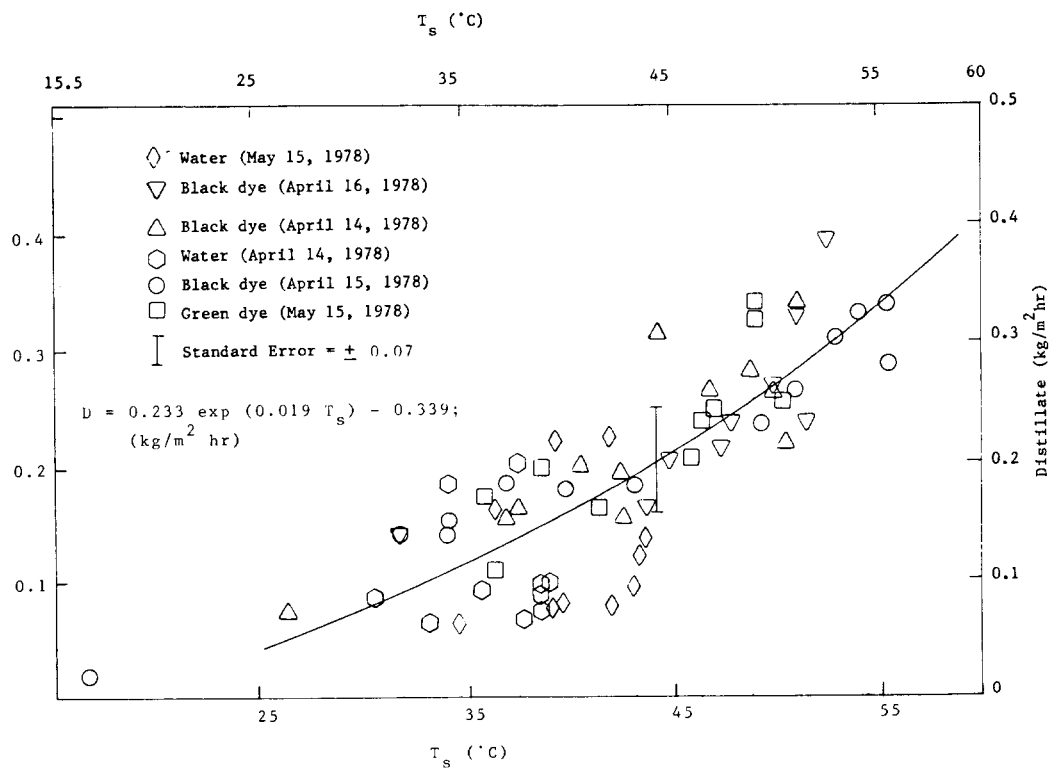

Fig. 10. Correlation of distillate output and T_s.

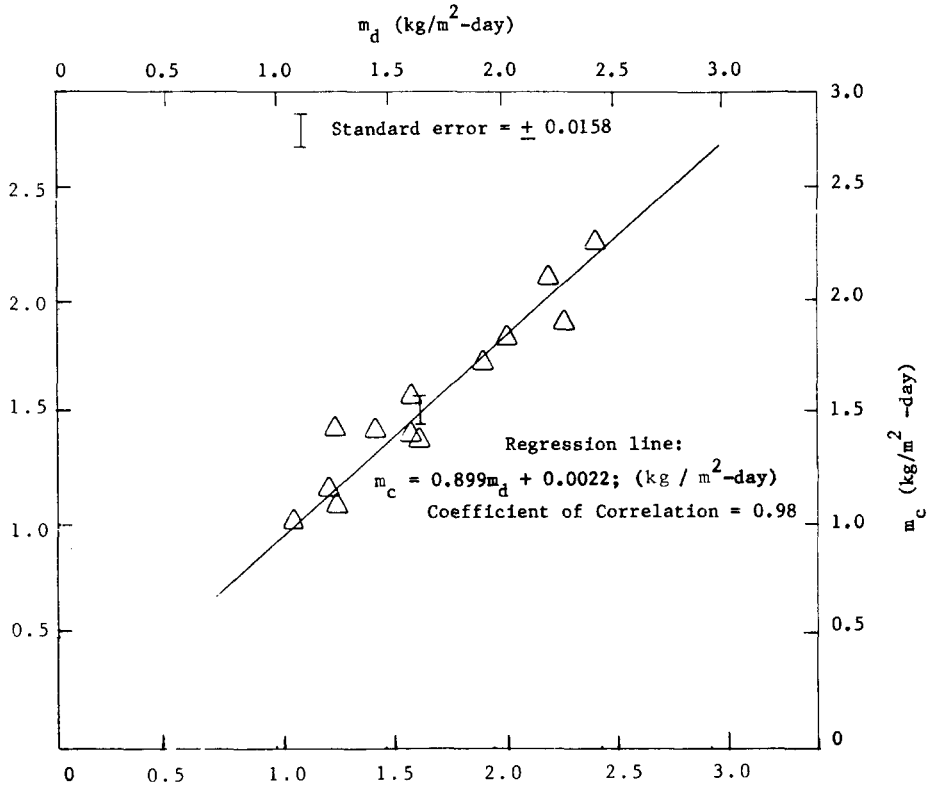

Fig. 11. Comparison of outputs of red dye (50 ppm).

and completely clear days, since on a completely cloudy day (when sun did not produce any shadow) there was no difference in distillate outputs from the two stills.

From these plots a scheme is developed so that the effect of a certain dye in increasing the evaporation can be calculated. It can be seen from the plots of regression lines for various dyes that the slope of the lines decreases as the dye changes from red to black. This is to be expected since black dye absorbs more radiation at the surface as compared to red dye and hence increases the output. This information is shown in Fig. 12, where slope S is plotted vs normalized absorption χ. χ is an indication of how well a dye solution absorbs solar radiation. The value of x^* in χ is taken to be 1.27 cm. Also plotted (see Fig. 13) is the relationship between slope S and intercept b of the regression lines for

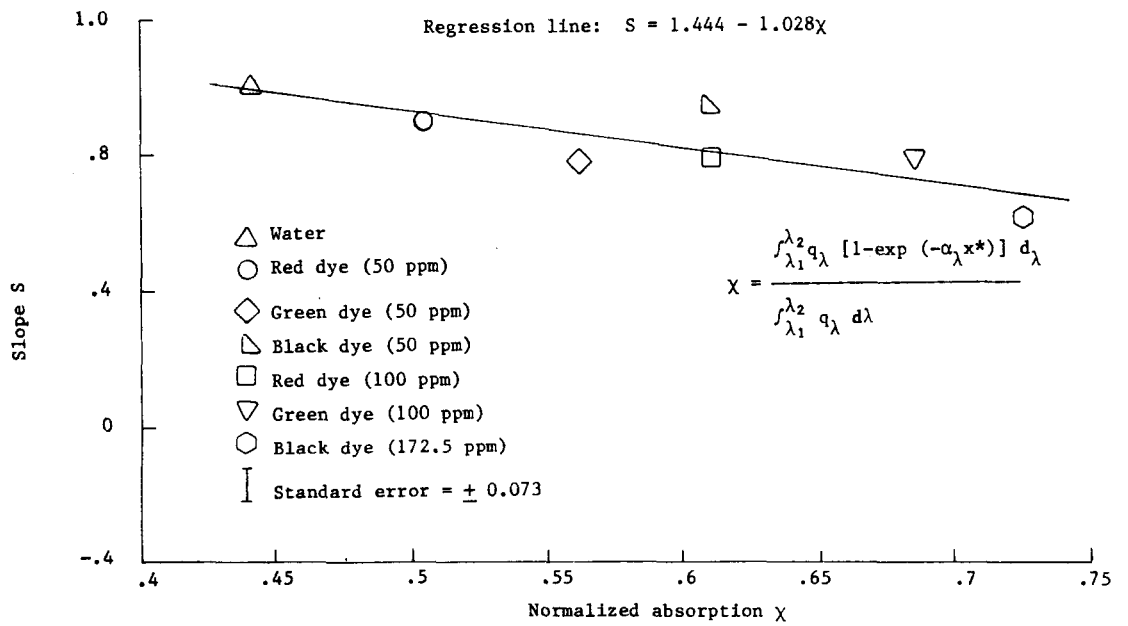

Fig. 12. Correlation of S and X.

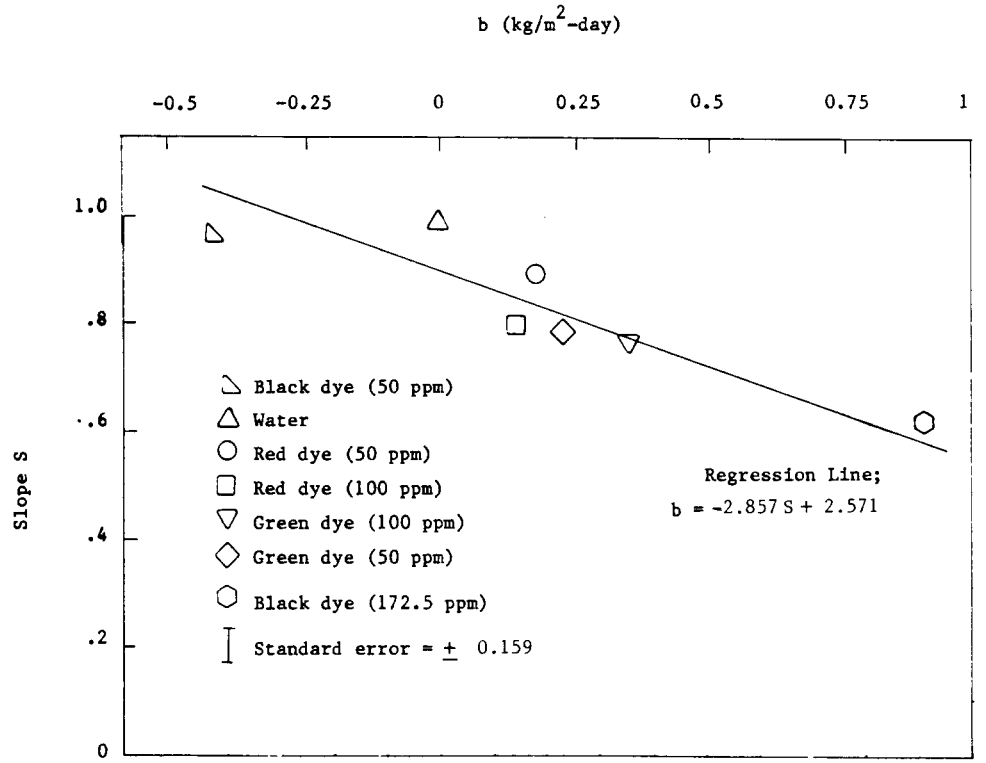

Fig. 13. Correlation of S and intercept b.

various dyes. Thus for any dye where χ is known (which can be found from its absorption spectrum) the percentage increase in evaporation I over that of controlled unit can be found by following equation:

$$I = \left\{\frac{1}{s}\left(1 - \frac{b}{m_c}\right) - 1\right\} \times 100 \text{ per cent.} \qquad (22)$$

It is evident from the above equation that I depends on different seasons since m_c is season dependent. The maximum of m_c is in June and minimum in December.

It is also instructive to ascertain whether there is any carry-over of the dye molecules in the distillate. From the absorptance spectrum of the distillate there is no evidence of such carry over[2]. This is to be expected since the maximum surface temperature recorded for the dye solution was 60°C where the boiling points of these dyes are of the order of 180°C and more[7]. Thus only water evaporates.

PART III

COMPARISON OF THEORETICAL AND EXPERIMENTAL RESULTS

Figure 14 shows a representative plot of the comparison between the theoretical and experimental temperature-time history of the various layers of the dye solution. As can be seen from this plot, the agreement between the two is excellent.

Similar plots for various days show the excellent correlation between experiment and theoretical prediction[2]. It is appropriate therefore to extrapolate on the model to investigate the effects of various parameters like ambient temperature, wind velocity and concentration of dye, on still productivity.

Effect of ambient temperature

The effect of various ambient temperatures for 6 March 1978 on distillate output is plotted in Fig. 15. The computer simulation based on the analytical model is done by increasing or decreasing the experimental ambient temperature-time history for the particular day by a fixed amount. Thus in Fig. 15 the temperature ratio is T_{sim}/T_{amb}, where T_{sim} is the modified temperature-time history used in the model. The simulations for each T_{sim}/T_{amb} ratio were done in thermal cyclic equilibrium such that steady state conditions for distillate output were achieved. This was done to eliminate the effects of capacitance of the still. As can be seen from Fig. 15, an increase of T_{amb} by 40 per cent increases the distillate output by 27 per cent. This result is to be expected because an increase in ambient temperature increases the surface temperature of the water thereby increasing the distillate output. This result is further enhanced by the fact that at higher ambient temperature the heat losses from sides and bottom of still are also reduced. The above result is also confirmed by other studies[8, 9].

Effect of wind velocity

The effect of wind velocity on distillate output for the still is plotted in Fig. 16. There is an increase of output by about 10 per cent with wind velocity increasing from 1 to 32 km/hr. This is because there is better heat transfer from the glass cover to the ambient. However, with increasing wind velocity (about 32 km/hr) the output

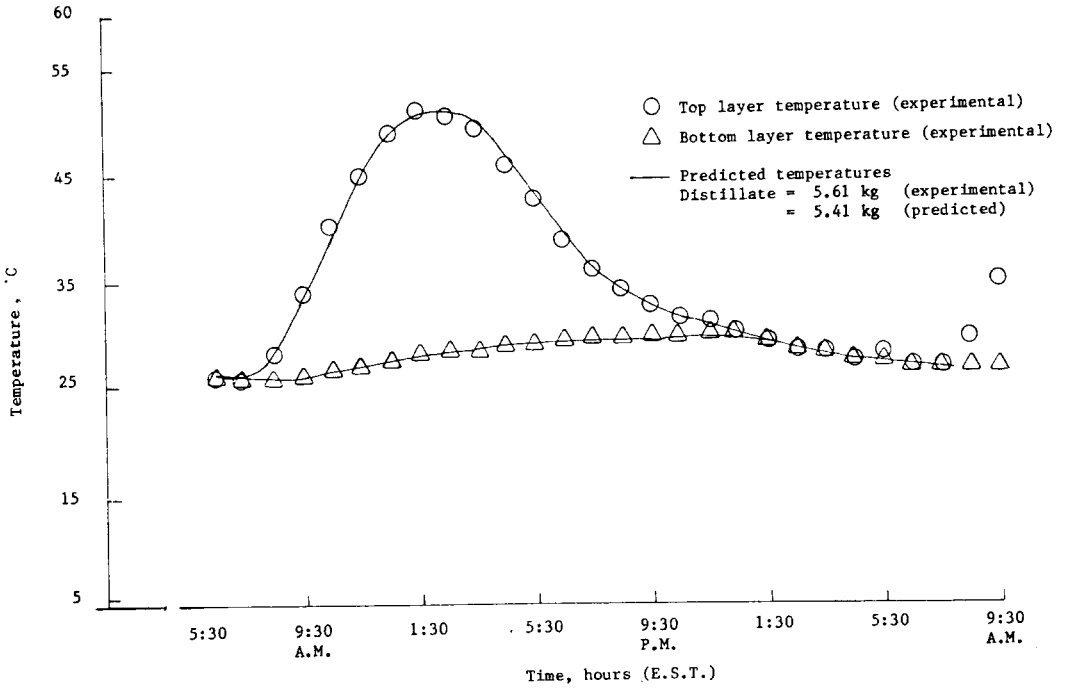

Fig. 14. Comparison between experimental and theoretical results for black dye (172.5 ppm); 14 April 1978.

starts leveling off. The reason for this is that at higher wind velocities the limitation on heat transfer is imposed by the conductance of glass and not by the outside heat transfer coefficient. It should be pointed out that there are conflicting results presented in literature on the effect of wind velocity on productivity[8]. However, some computer simulation results[9] do confirm the increase of productivity with increasing wind velocity.

Effect of dye concentration

Figure 17 shows the computer simulation results of the effect of various dyes and their concentrations on the

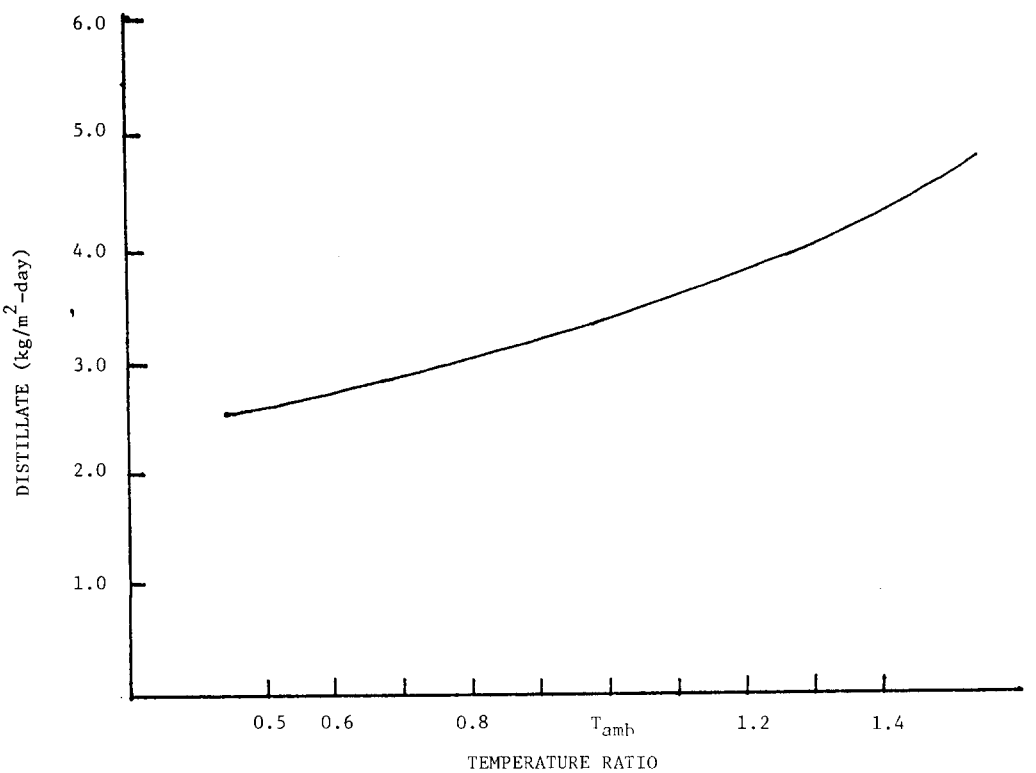

Fig. 15. Analytical plot of the effect of ambient temperature on distillate output; 6 March 1978.

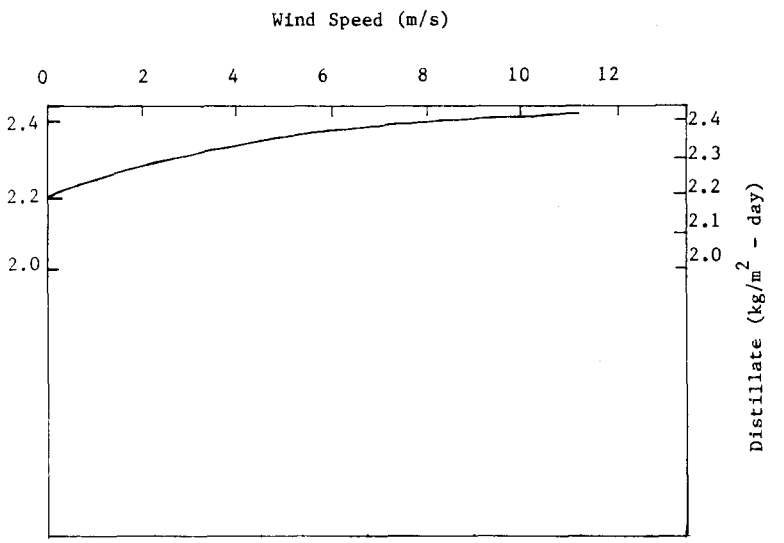

Fig. 16. Analytical plot of the effect of wind speed on distillate output; 6 March 1978.

still productivity. It should be mentioned again that in the computer program all the environmental parameters were the same for each dye concentration run and the still was simulated in thermal cyclic equilibrium. However, the dye concentration was "changed" by increasing or decreasing the data for α_λ in the program. At zero ppm concentration they have the same output, and as the dye concentration increases, different dye-water systems exhibit different outputs with black having the maximum distillate while red has the lowest for the same concentration. This is because of better absorption of solar energy by black dye as compared to red. However, after about 500 ppm, there is no difference in distillate outputs from various dyes, since around this concentration level about 99.9 per cent of the incoming solar radiation is absorbed in the first 1.27 cm layer of dye solution, thus making the evaporation independent of the nature of dye. It is also instructive to look at the surface temperature and bottom layer temperature-time histories for black dye with 50 and 400 ppm concentrations (Fig. 18). Besides the higher surface temperature for 400 ppm concentration, an interesting point can be seen in the bottom layer temperatures for the two concentrations. The maximum variation in bottom layer temperature for 400 ppm concentration is about 1°C while for 50 ppm concentration is about 4°C. These temperature variations are an indication of heat losses from the bottom and sides of the still, which are ultimately reflected in the productivity of the still. The above point is an indication of the effect of depth of the dye-water system on productivity, since by

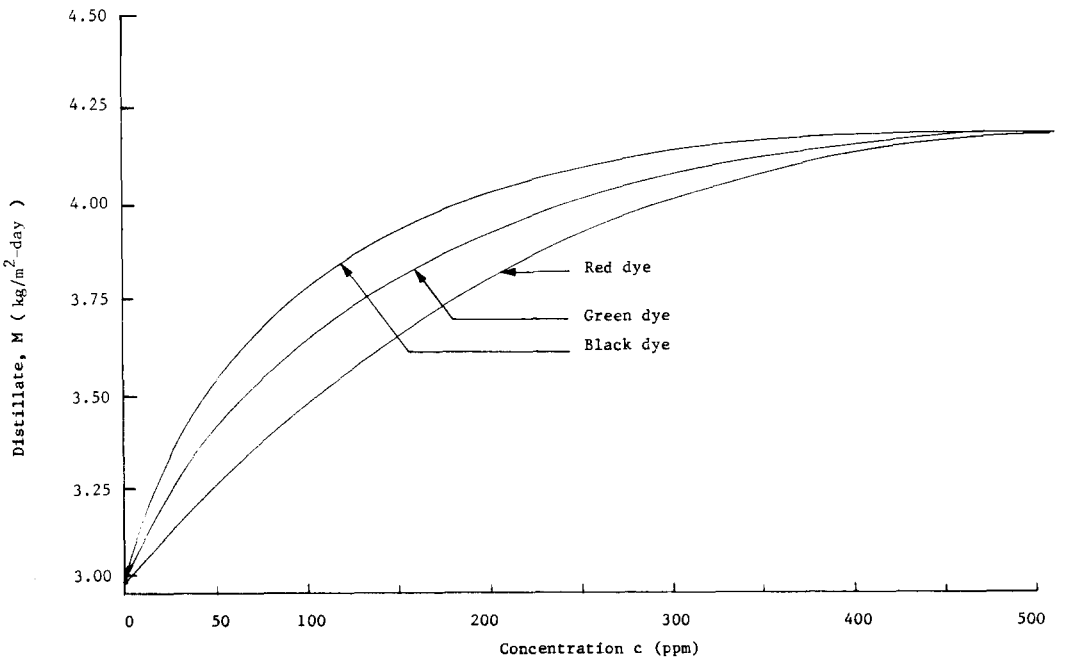

Fig. 17. Analytical plot of the effect of dye concentration on distillate output; 14 April 1978.

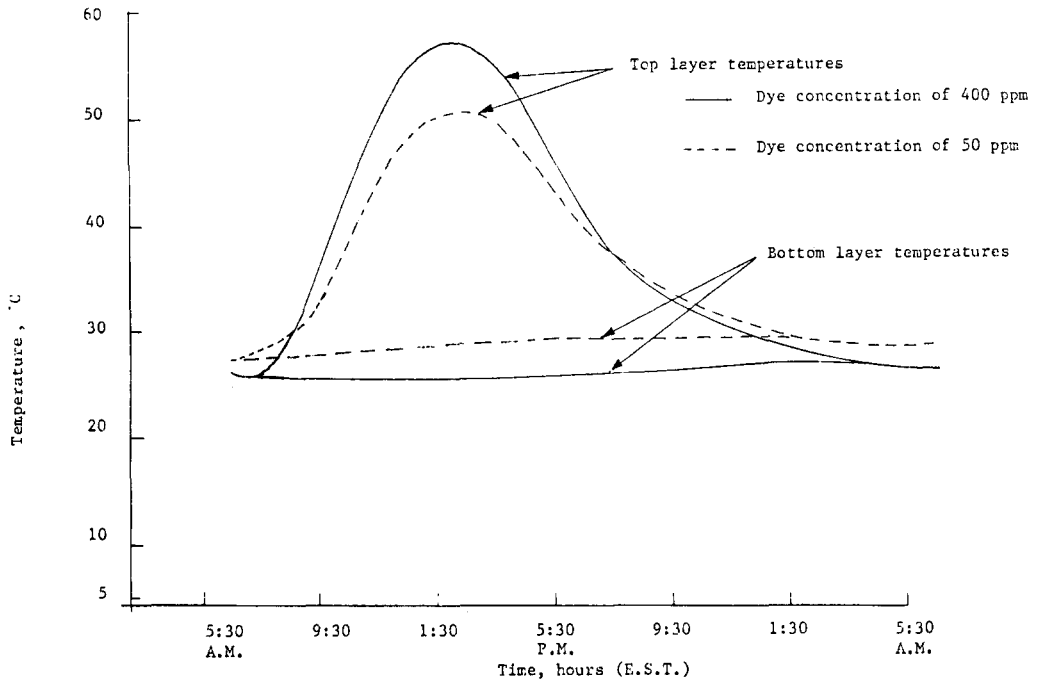

Fig. 18. Analytical plot of the temperature-time history for black dye; 14 April 1978.

increasing the concentration of dye, the effective depth of the still is increased, while, with decreasing concentration of the dye, the depth is decreased. Thus, it can be concluded that for the same concentration of dye, increasing the basin depth will increase the productivity. In fact, it can be shown that if the depth of the basin is greater than 15 in., then the bottom layer temperature remains unchanged for 24 hr cycle [2].

From Fig. 17 it can be seen that the distillate output M follows the law of diminishing returns and thus it is not advantageous to use greater concentrations of dye after about 400 ppm. Moreover, greater concentration of dye increases the cost of distillation. Thus, it is useful to develop a function that is able to give an optimum concentration of a particular dye, taking into consideration the above points. Such a function would take into account the two counteracting parameters, (dM/dc) (which decreases with concentration of dye) and M

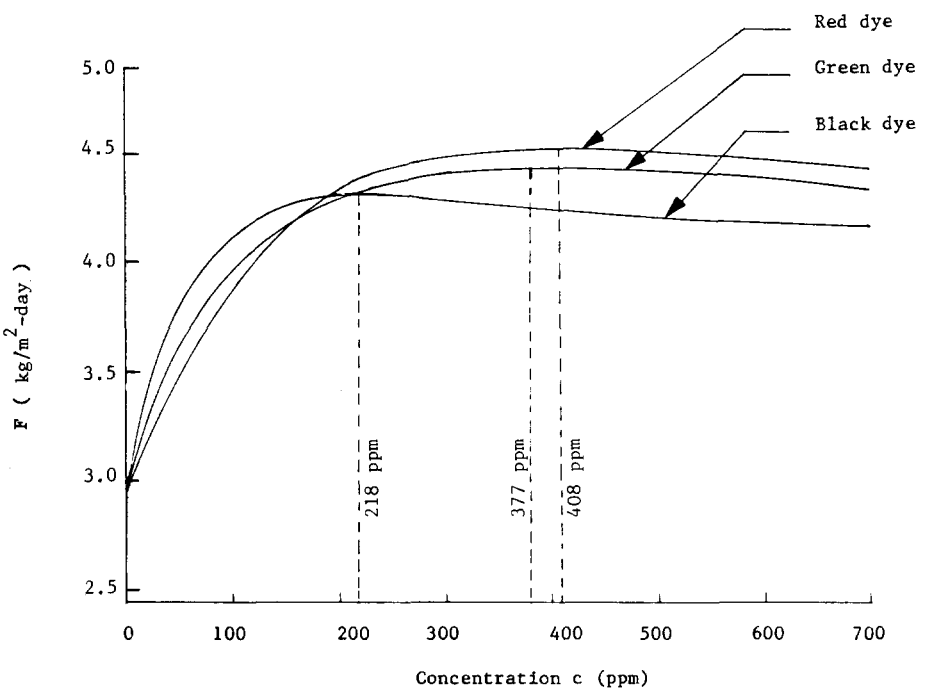

Fig. 19. Optimum concentrations for different dyes on a typical spring day at Gainesville, Florida.

(which increases with c). In order to have these two quantities expressed in the same units, is multiplied by the concentration c. This then yields the following function F:

$$F = c\frac{dM}{dc} + M. \quad (23)$$

This function F is plotted vs concentration (Fig. 19) and gives an estimate of the optimum concentrations for various dyes.

CONCLUSIONS

The following conclusions can be drawn from the present investigation;

(1) Addition of water soluble dyes increases the productivity of deep basin solar still by as much as 29 per cent (for black dye with concentration of 172.5 ppm), over that from the control unit.

(2) Among the dyes tested, black napthylamine dye is most suitable both from the point of view of increasing evaporation and lightfastness.

(3) Based upon experiments, a simple method of calculating percentage increase in evaporation by using a dye over that from the control unit has been developed.

(4) There is an excellent agreement between the results of the analytical model and the experiments.

(5) The analytical model predicts an increase in distillate output with increasing ambient temperature. It also predicts an increase in still productivity with increasing wind speed.

(6) The analytical model also predicts the increase of distillate with increasing concentration of dye up to 500 ppm, after which it is independent of the concentration.

(7) An analytical method of predicting an optimum concentration of a particular dye is developed. The optimum concentration for a dye is obtained where the function F (eqn 23) is maximum.

Acknowledgements—The author wishes to thank Solar Energy and Energy Conversion Laboratory at the Univ. of Florida for the financial help during the course of this study. Thanks are also due to Dr. R. Pagano for his critical reading of the manuscript.

NOMENCLATURE

A area of layers, m^2
A_c area of still cover, m^2
A_g area of glass cover, m^2
b intercept of regression lines, kg/m^2-day
c concentration of dye, ppm
c_{pg} specific heat of glass, kJ/kgK
c_p specific heat, kJ/kgK
C constant in eqn (5)
D_{ij} binary diffusion coefficient, m^2/sec
F factor given by eqn (19), kg/m^2-day
F_e, F_a emissivity and geometrical shape factors
g acceleration due to gravity, m/sec^2
Gr Grashof number
h_c convection heat transfer coefficient from water surface to glass cover, W/m^2K
h_{evap} evaporation heat transfer coefficient, W/m^2K
h_{fg} enthalpy of vaporization for water, kJ/kg
h_m mass transfer coefficient, kg/m^2hr
h_0 outside heat transfer coefficient, W/m^2K
I percentage increase in evaporation
k_e equivalent conductivity, W/mK
k_{pg} thermal conductivity of Plexiglas, W/mK
k_w thermal conductivity of water, W/mK
$k_{w/a}$ thermal conductivity of air–water mixture, W/mK
ℓ thickness of layer for convection heat transfer in dye-water solution, m
ℓ^* thickness of layer shown in Fig. 1
$m_{i,j}$ mass fraction of species i near surface j
m_c distillate output from control unit, kg/m^2-day
m_d distillate output from still with dye, kg/m^2-day
M distillate output, kg/m^2-day
M_{air}, M_w molecular weight of air and water respectively
Nu_m mass transfer Nusselt number
n_1 index of refraction for air–water vapor mixture
n_2 index of refraction for dye-water solution
P perimeter of the still, m
P_{atm} atmospheric pressure, N/m^2
Pr Prandtl number
P_{ws}, P_{wg} partial pressure of water near water surface and glass respectively, N/m^2
q_λ spectral solar energy flux, kW/m^2-μm
$q_\lambda(t)$ spectral solar radiation on a horizontal surface, kW/m^2-μm
$q_\lambda^0(t)$ spectral solar radiation passing the air–water interface, kW/m^2-μm
$q_{\lambda,i}^n(t)$ spectral solar radiation incident on layer n
$q_s(t)$ incident solar radiation on glass cover, kW/m^2
$q(t)$ total solar radiation on horizontal surface, kW/m^2
r reflectance
Ra_ℓ Raleigh number
S slope of the regression lines
Sc Schmidt number
T_{al} temperature of aluminum cover, °C
T_{amb}, T_∞ ambient temperature, °C
T_b temperature of the bottom of the basin at time t, °C
T_H, T_C temperature of hot and cold layer, respectively, °C
$T_{n,max}$ maximum temperature of layer n, °C
T_n^t temperature of layer n at time t, °C
T_{n+1} temperature of layer $n+1$, °C
T_s, T_g temperature of the water surface and glass cover, respectively, °C
T_{sky} apparent sky temperature, °C
U overall heat transfer coefficient between water and environment, W/m^2K
α_w thermal diffusivity of water, m^2/sec
α_g solar absorptivity of glass
α_λ absorption coefficient of the dye solution, m^{-1}
β thermal coefficient of volume expansion, K^{-1}
Δt time interval, hr
Δx thickness of layer, m
Δx_g thickness of glass cover, m
Δx_{pg} thickness of Plexiglas basin, m
Δx^* path length of incident solar radiation ray in a layer, m
$\Delta\rho$ density difference of the moist air between water surface and glass cover, kg/m^3
$\zeta(t)$ dimensionless parameter in eqn (16)
χ normalized absorption
λ wavelength, μm
λ_1, λ_2 upper and lower limits of wavelengths of solar spectrum, μm
η efficiency of distillation
ν_w kinematic viscosity of water, m^2/sec
ν_m kinematic viscosity of air–water vapor mixture, m^2/sec
σ Stefan–Boltzman constant, appropriate units
$\bar{\tau}_{g/w}$ average transmittance of condensate covered glass
θ_i, θ_r angle of incidence and refraction at air–water interface, degrees
ρ density of fluid, kg/m^3
ρ_w density of water, kg/m^3

REFERENCES

1. S. G. Talbert, J. A. Eibling, G. O. G. Lof, C. Wong and E. N. Sieder, *Manual on Solar Distillation of Saline Water,*

Research and Development Program Rep. 546. U.S. Dept. of Interior (1970).
2. A. K. Rajvanshi, Analytical and experimental investigation of the effect of dyes on solar distillation. Doctoral dissertation, Dept. of Mechanical Engineering, University of Florida (1979).
3. E. R. G. Eckert and R. M. Drake, *Analysis of Heat and Mass Transfer*. McGraw-Hill, New York (1972).
4. D. K. Edwards, V. E. Denny and A. F. Mills, *Transfer Processes*. McGraw-Hill, New York (1976).
5. J. L. Threlkeld and R. D. Jordan, Direct solar radiation available on clear days. *ASHRAE Trans.* **64**, 45–53 (1958).
6. G. M. Hale and M. R. Querry, Optical constants of water in the 200-nm to 200-μm wavelength region. *Appl. Optics* **12**(3), 555–563 (1973).
7. K. Venkataraman, *Chemistry of Synthetic Dyes*, Vol. I. Academic Press, New York (1952).
8. G. O. G. Lof, J. A. Eibling and J. W. Bloemer, Energy balances in solar distillers. *AICHE J.* **7**(4), 641–649 (1961).
9. P. I. Cooper, Digital simulation of transient solar still processes. *Solar Energy* **12**(3), 333–346 (1969).